

THE APPLICATION OF PHOTON CORRELATION LASER VELOCIMETRY  
TO TURBULENT FLOW FIELD INVESTIGATIONS

G. D. Catalano  
Louisiana State University  
Baton Rouge, Louisiana

H. E. Wright  
Air Force Institute of Technology  
Wright Patterson AFB, Ohio

### Abstract

A laser velocimeter with photon correlation processing scheme used to investigate various turbulent flow fields. Naturally occurring contaminant serves as scattering centers for the experiments. The photon correlation technique is tested for its sensitivity to laser incident intensity, and response to flow unsteadiness. In addition, a test configuration which features high shear regions and significant reverse flow is also investigated. An improved method for the calculation of the turbulent intensities from the correlation curves is presented and examined. A direction for future interpretation of photon correlation data is proposed. Actual real world engineering applications where turbulent velocity data is required are discussed.

### I. Introduction

Within the past few years, the commercial availability of fast digital correlators has led to new technologies of measurement based upon the quantum resolved properties of low light level. The digital or photon correlation processing technique used in laser velocimetry applications has remarkable power in that it covers a wide dynamic range, is sensitive to extremely low scattered light intensities and does not require a continuous signal. The requirement for low light levels permits the researcher to employ relatively small lasers (e.g. 5-15 mW) and the use of naturally occurring contaminant as the scattering centers. However, there are drawbacks to the correlation technique such as serious problems with flare and ambient light, the photon pile-up phenomenon, little control over the size distribution of the scattering centers, only ensemble average data retrievable, and the mean velocity and the turbulent intensity information alone calculable from the correlation function. The purpose of this report is to document the experiences gained by the authors with the photon correlation technique as it applies to the measurement of turbulent flow fields. In concert with the experiences, several new data analysis algorithms are presented.

### II. Experimental Approach

In order to establish the credibility of the photon correlation processing technique using the Malvern 50 ns unit, the first segment of the experimental investigation focussed on measuring the turbulent flow field of a rectangular nozzle free jet [1]. The rectangular jet was chosen because considerable hot wire anemometry obtained data already existed and thus a comparison was realizable. The exit plane velocity varied from 130 m/sec to 260 m/sec. Measurements of the mean

velocities and the turbulence intensities were made at various downstream locations. Examples of the data are shown in Figures 1 and 2. For this experiment, the naturally occurring contaminant found in the laboratory compressed air supply was used as marking particles. The data presented in Figure 2 points out one of the drawbacks of the 50 ns unit. The experimenter has the choice of being able to measure high subsonic speeds in the central region of the jet or measuring turbulent intensities in high shear regions. The existence of this dilemma is due to required beam spacing for the inclusion of the phase modulator in the laser velocimeter optical set-up. The spacing then limits to a large extent the angle of intersection between the two laser beams.

The second step involved measuring the flow field entering the combustion chamber of an actual jet engine [2]. Once again, comparison was made to hot wire anemometry data when available. In addition to the practical engineering significance, the long inlet duct provided regions of relatively large flow accelerations and decelerations (Figure 3). This would enhance the understanding of the sensitivity of the photon correlation scheme to particle size biases. In fact, this portion of the investigation led to effort being concentrated in the area of particle dynamics [3]. For the inlet duct flow, the air supply was the frequently not-too-clean Dayton atmosphere present outside the jet engine test facility. No additional scattering centers were introduced. Typical results are shown in Figures 4 and 5.

Difficulties in properly seeding flows behind blunt or bluff bodies led to the next investigation [4]. The flow field chosen was a subsonic jet impinging upon a flat disc. Laboratory compressed air without additional scattering particles was used. Velocity measurements were then made behind the disc in the wake region at various downstream locations. Figures 6 and 7 present examples of the mean velocity and turbulent intensities measured.

A quantification of the sensitivity of the photon correlation scheme to incident laser intensity was the next goal [5]. The approach taken was to vary the actual size of the laser beam by means of a beam expander/aperture arrangement. The  $1/e^2$  beam diameter was varied from 0.5 mm to 10 mm. The resultant varying sized control volumes are located in the flow field of the previously discussed rectangular nozzle turbulent free jet. Mean velocities and turbulent intensities were then calculated from the resultant correlation curves (Table 1).

Mean velocities and turbulent intensities in the near field region of the wake flow behind a

circular disc immersed in a turbulent jet flow are obtained. Figure 6 presents mean velocity profiles for various downstream locations.

With the application of the photon correlation processing technique to a flow field located in the test section of the wind tunnel, problems concerning ambient and/or flare light and photon pileup arose. The manifestation of these problems often is that the expected damped cosinusoidal correlation function is skewed and/or distorted. This makes it very difficult to obtain credible mean velocity or turbulent intensity data. An approach [6] was devised based on polynomial curve fitting procedure and applied to a two dimensional turbulent wake flow field. Figures 8 through 11 indicate the correlation functions prior to and after the correction procedure has been employed. Once the credibility of the correction procedure had been established, the near field of the two dimensional wake was documented in detail [7].

Typical results are presented in Figures 12 and 13. For this investigation, the free stream velocity and the Reynolds number based on cylinder diameter are 5.9 m/sec and approximately 50,000 respectively. The cylinder was tested with a stationary ( $w = 0$  RPM) and a rotating ( $w = 500$  RPM) initial condition.

A flapping (oscillating) jet allowed the sensitivity of the photon correlation scheme to an unsteady flow field to be documented. The nozzle design employed consists of a modified fluidic element with a feedback mechanism [8]. For this experiment, a centrifugal blower was employed with the naturally occurring contaminant serving as the light scatterers. Mean and turbulent velocity profiles are presented in Figures 14 and 15.

The most recent application of the photon correlation laser velocimeter has been in the turbulent flow field associated with a thrust augmenting ejector wing design. The two dimensional model consists of two subsonic airfoils with an ejector nozzle/constant area duct [9] (Figure 16). The intent of the investigation was to determine the effects of an ejector on the flow characteristics around the airfoil(s) specifically with respect to supercirculation and, thus, increased lift. A thorough documentation was performed [10]. Typical results are shown in Figures 17 through 19. The ratio of the ejector velocity to free stream velocity was kept constant and equal to 2.0. Here, once again, naturally occurring contaminant present in the tunnel/ ejector flow served as scattering centers.

### III. Experimental Results and Discussion

The investigation of the rectangular nozzle turbulent jet both established the credibility of using the photon correlation processing technique with its inherent advantages of low laser intensity and no artificial seeding but also it pointed out one significant drawback (Figures 1 and 2). Whereas with a counter or tracker processor, a Bragg cell can be used to shift the frequency of the laser light up to 40 MHz, the photon correlator requires the use of a phase modulator which has an upper limit frequency shift equal to approximately 2 MHz. Thus, a serious problem arises when the flow is both high in mean velocity and in turbulent intensity. The mean velocity data can

be obtained but at the expense of any turbulence information.

The flow geometry in the inlet duct for a jet engine is shown in Figure 3.

Figure 4 presents mean velocity profiles for the flow location downstream from the venturi. Note the uniformity of the flow in the center of the duct. The flow field measured by the laser velocimeter seems to be somewhat wider than that measured by the hot wire. This trend is apparent in several additional profiles not presented and is principally due to the optical arrangement with the collecting lens being in the same plane as the beam intersection.

An additional comment should be made concerning the comparison of the mean velocity profiles downstream from the venturi. Though the shapes for the LV and hot wire data are similar, the absolute velocities at the centerline are 3.6 and 6.4 m/sec lower using the hot wire anemometer for 50 percent and 70 percent throttle respectively. These variances represent approximately 10 percent of the measured mean velocity, and are due to the relatively large size particles in the air (i.e. approximately 5-10 microns in diameter).

The lateral distributions of the turbulence intensities,  $u'^2/U^2$ , are plotted versus lateral displacement from the centerline,  $y/r_0$ , in Figure 5. Note that near the centerline, the LV seems to indicate zero turbulence level. In fact, the photon correlation scheme is not well suited for determining turbulence intensities for nearly laminar flow. Again note that the LV measured flow fields seem wider for the different locations.

For the disc immersed in a turbulent jet (Figures 6 and 7), it is possible to use the natural scatterers and obtain meaningful data. The local mean velocity,  $U$ , is plotted versus non-dimensionalized lateral displacement from the disc center,  $Y/R$  where  $R$  is the disc radius. At the centerline of the flow field (i.e.  $Y/R=0$ ), the flow initially accelerates in a negative  $X$  direction, then decelerates and finally accelerates in a positive downstream location. Note that the maximum negative mean velocity is not reached until the downstream location  $X/R=1.50$ . The maximum width of the recirculation region is approximately 3.5 diameters. The local turbulence intensity varies between 0.20 and 0.40 with the largest magnitude being reached at  $X/R=1.50$  near the flow centerline (Figure 7).

The non-dimensionalized wake momentum thickness,  $\theta_0/2R_0$ , calculated by integrating the momentum equation over the flow cross section is plotted versus non-dimensionalized downstream location,  $X/2R_0$  in Figure 12. The values plotted for the rotating case, which are consistently larger for  $X/2R_0 \leq 0.75$ , represent the sum of the momentum thickness above the cylinder centerline (i.e. rotation in the direction of the flow) and below the cylinder centerline (i.e. opposite of the rotation direction). The momentum thickness is asymmetric for  $w = 500$  rpm. Consider a kinetic perspective. The rotation creates an asymmetric pressure distribution around the cylinder, which coupled with the uniform flow produces a Magnus-type or lift force. The associated

increment in the drag is manifest in the increase in the value of  $\delta$ .

The mixing width,  $Y_{1/2}$ , non-dimensionalized by  $\theta_0$  is plotted versus non-dimensional distance downstream,  $X/\theta_0$ , in Figure 13. As is the case for the momentum thickness,  $Y_{1/2}$ , for  $\omega = 500$  rpm, is consistently larger after the initial flow development. The mixing width is a possible length scale with which to describe the flow field and is related to the slope of the mean velocity profile. In the recirculation region, the cross stream momentum advection term ( $V\partial V/\partial y$ ) is much larger than for the fully developed case. The associated transverse flow strain rate would tend to compress eddies in the cross-stream direction and thus result in a decrease in the magnitude of a characteristic length scale. This is a possible explanation for the initial decrease in  $Y_{1/2}$ .

The photon correlation processing technique was shown to be quite insensitive to incident laser intensity (Table 1). The unfocussed laser beam diameter is 1.1 mm. For diameters up to 7 mm, the measured mean velocity varies by less than 5%. The error begins to grow more rapidly for the larger beam diameters. An interesting occurrence is that the measured mean velocity has the greatest magnitude for the largest size beam diameter. This phenomenon which is repeatable is directly opposite to the trend observed when tracking or counting signal processing is used. The data for the half-widths shows a similar behavioral pattern.

In Figure 14(a) the value of the mean velocity,  $U$ , in the  $x$  direction is plotted versus oscillation frequency,  $f$ , for several downstream locations. The mean velocities shown are taken at the jet/nozzle centerline (i.e.  $y = z = 0$ ). Notice that as the oscillation frequency is increased from  $f=4$  hz to  $f=18$  hz, the measured mean velocity also increases. In fact, as the frequency increases from 8 hz to 18 Hz,  $U$  varies almost linearly with  $f$ .

In Figure 14(b) the mean velocity,  $U$ , at the vertical location,  $y = 1.90$  cm or  $y/2r_0 = 1.5$  is plotted for the various frequencies and downstream locations. Note that while there still is a nearly direct relationship between increasing  $f$  and thus resulting in the net increase in  $U$ , the functional dependence is not as strong as is the case for  $y/2r_0 = 0$ .

Turbulent intensities in the longitudinal direction,  $(u^2)/U$ , plotted versus oscillation frequency are shown in Figures 15(a) and 15(b) for several different downstream locations. For both  $y/2r_0 = 0$  (Figure 15(a)) and for  $y/2r_0 = 1.50$  (Figure 15(b)), the value of the turbulence intensity is clearly not a simple function of the oscillation frequency. It is evident that the potential core region which typifies the near field of a classical turbulent jet does not exist for the oscillating jet. In fact at  $x/2r_0 = 2$  and  $y/2r_0 = 0$ , the turbulence intensity ranges from 0.10 to 1.58 as the oscillation frequency is increased.

In Figure 16, the location of the mean velocity and turbulent intensity data obtained are shown for the ejector wing experiment. Note that in all cases,  $x$  is measured, longitudinally, from

the leading edge and  $z$  is measured vertically from the airfoil surfaces.

Figure 17 shows mean velocity profiles upstream of the ejector wing. The effect of the ejector in the mean velocity profiles is to accelerate the mean flow above the upper surface and to decelerate the mean flow beneath the ejector wing. This effect is quite pronounced immediately upstream of the leading edge.

Mean velocity and turbulent intensity profiles are shown for the downstream location  $x/c = 0.2$ , in Figure 18. The mean flow is consistently faster in the ejector powered case. The value of the turbulent intensities reduce to the free stream value closer to the wing surface with the ejector working. This would indicate a shift of the potential flow down toward the upper surface.

The mean and turbulent velocity field downstream of the ejector nozzle is examined in Figure 19 for  $x/c = 0.58$ . Note that the flow for both cases actually accelerates after it enters the constant area mixing duct. Also consider the relatively high turbulent intensities in the confining duct for the ejector powered case. Value of  $u_{rms}/U$  equal to 0.30 are measured which is indicative of jet mixing rather than characteristic of duct type flow.

Bendat and Piersol [12] have developed the notion of partial coherence functions which can help establish the cause of a linear dependence indicated by an ordinary coherence function. Consider the application of partial coherence functions to photon correlation spectroscopy.

Defining  $R_1$  as the finite fourier transform (FT) of the autocorrelation function  $r_{11}$  where

$$r_{11}(\tau) = \lim_{T \rightarrow \infty} \frac{1}{T} \int_0^T u_1(x,t) u_1(x,t+\tau) dt$$

and

$$R_2 = FT\{r_{22}\}$$

$$R_c = FT\{r_{12}\}$$

then (Figure 20)

$$R_{2 \cdot 1} = R_2 - L_{12} R_1 = R_2 - \left(\frac{S_{12}}{S_{11}}\right) R_1$$

$$R_{c \cdot 1} = R_c - L_{1c} R_1 = R_c - \left(\frac{S_{1c}}{S_{11}}\right) R_1$$

where  $R_{2 \cdot 1}$  denotes the finite fourier transform over long record length of input  $r_{22}$  with linear effects of  $r_{11}$  removed from  $r_{22}$ . Here  $S(f)$  denotes the autospectral or cross-spectral density function. The partial coherence function can then be defined as

$$\gamma_{c \cdot 1}^2 = \frac{S_{c \cdot 1}^2}{S_{22 \cdot 1} S_{cc \cdot 1}}$$

where

$$S_{22 \cdot 1} = \frac{\text{Expected Value of } [R_{2 \cdot 1}^* R_{2 \cdot 1}]}{T}$$

and similarly for  $S_{cc \cdot 1}$ .

The implications of this type of analyses are quite straightforward. The photon correlation spectroscopy technique permits the experimenter to calculate the classical turbulence scalar correlation functions. The use of partial coherence will then help establish the relationship between the scalar functions. Any degree of non-linearity (i.e. noise) in the transformation will be clearly identified.

#### IV. Conclusions

The photon correlation processing scheme proved to have several major advantages and disadvantages. The use of naturally occurring contaminant as the light scattering centers permitted experiments to be set up and data obtained fairly rapidly since no artificial seeding was required. Additionally, the technique was shown to be fairly insensitive to laser incident intensity as the control volume size was varied by more than an order of magnitude with no discernable effect on the data. Problems can and did arise with the response of the naturally occurring contaminant specifically in regions of high flow acceleration and deceleration, such as in the jet engine inlet duct. However, the photon correlation scheme permits the application of laser velocimetry to flow fields such as the near field wake region, and internal aerodynamic configurations which would have been exceedingly difficult to investigate using a processing scheme requiring artificial scatterers.

#### References

- [1] Catalano, G. D., Wright, H. E., and Cerrulo, "Photon Correlation Laser Velocimeter Measurements in Highly Turbulent Flow Fields," AIAA 18th Aerospace Sciences Meeting, Pasadena, CA, 14-16 January 1980.
- [2] Catalano, G. D., Wright, H. E., Rogers, H., Rivir, R., Viets, H., and Pratt, M., "Steady and Unsteady Turbulence Measurements Using a Photon Correlation Laser Velocimeter," 4th International Conference on Photon Correlation Techniques in Fluid Mechanics, Standord, CA, 24-27 August 1980.
- [3] Catalano, G. D., "Marker Particle Velocity Perturbations in Compressible Flows Over a Wavy Wall," AIAA Journal, Vol. 18, No. 10, pp. 1270-1272, Oct. 1980.
- [4] Catalano, G. D., Wright, H. E., "Turbulence Measurements Behind a Bluff Body," AIAA/AFIT Minisymposium, Wright-Patterson AFB, Ohio, 25 March 1981.
- [5] Catalano, G. D., Hamid, I., Wright, H. E., "Effect of Test Rhombus Size on Photon Correlation Laser Velocimeter Data," AIAA/AFIT Minisymposium, Wright-Patterson AFB, Ohio, 25 March 1981.

- [6] Catalano, G. D., Walterick, R. E., and Wright, H. E., "Improved Measurement of Turbulent Intensities by Use of Photon Correlation," to be published in AIAA Journal, March or April 1981.
- [7] Catalano, G. D., Walterick, R. E., and Wright, H. E., "The Near Field Two Dimensional Wake with Rotation and a Turbulent Ambient Stream" AIAA 14th Fluid and Plasma Dynamics Conference, Palo Alto, CA, 23-25 June 1981.
- [8] Catalano, G. D., Elrod, W. C., Viets, H., and Wright, H. E., "Photon Correlation Laser Velocimeter Measurements in an Unsteady Jet," presented at 53rd Meeting of the Supersonic Tunnel Association, NASA-Ames, CA, 26-28 Mar. 1980.
- [9] Viets, H., "Flip-Flop Jet Nozzle," AIAA Journal Vol. 13, No. 10, Oct. 1975, pp. 1375-1379.
- [10] Catalano, G. D., Nagaraja, K., Walterick, R. E., and Wright, H. E., "Turbulence Measurements in an Ejector Wing Design," AIAA Aircraft Systems and Technology Meeting, Dayton, Ohio, 11-13 August 1981.
- [11] Pike, E. R., "The Application of Photon Correlation Spectroscopy to Laser Doppler Measurements," Journal of Physics D: Applied Physics, Vol. 5, 1972, L23-25.
- [12] Bendat, J. S., and Piersol, A. G., Engineering Applications of Correlation and Spectral Analyses, Wiley & Sons, New York, 1980, pp. 220-233.

Table 1:

Laser Beam Diameter (mm)	U/U <sub>exit</sub>	$Y_{\frac{1}{2}}/Y_{\frac{1}{2}} @ 1.1 \text{ mm}$
1.1	.607	1
0.5	.606	1.09
1.0	.620	.99
3.0	.630	1.07
5.0	.580	.99
7.0	.563	1.27
10.0	.687	1.30

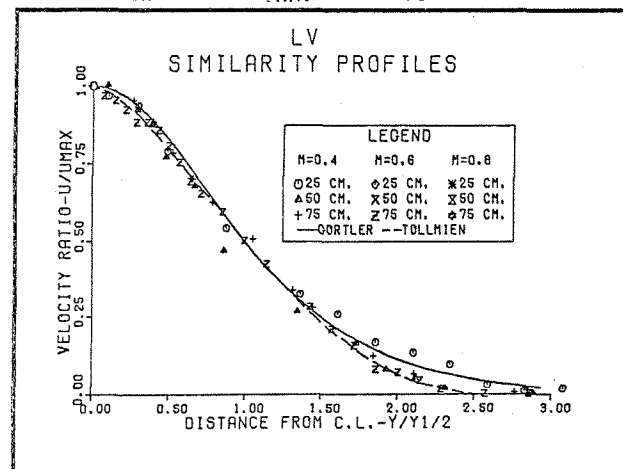


FIG. 1 LV MEAN VELOCITY SIMILARITY PROFILES

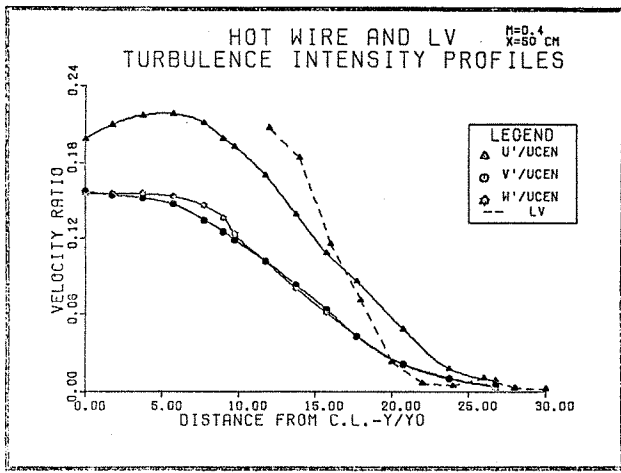


FIG. 2 HOT WIRE AND LV TURBULENCE INTENSITY AT  $M=0.4$  AND 50 CM

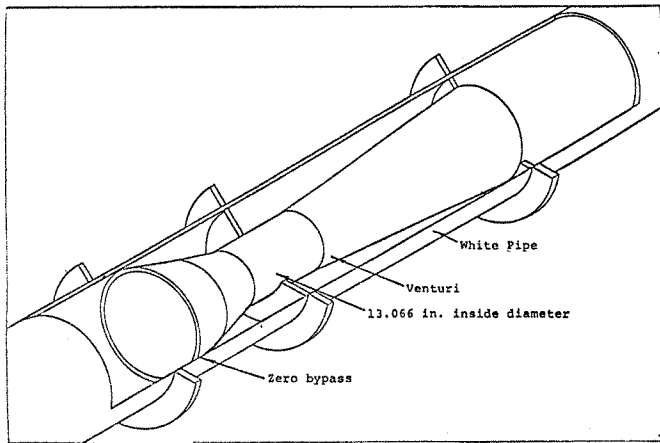


Figure 3. Inlet Duct Flow Configuration

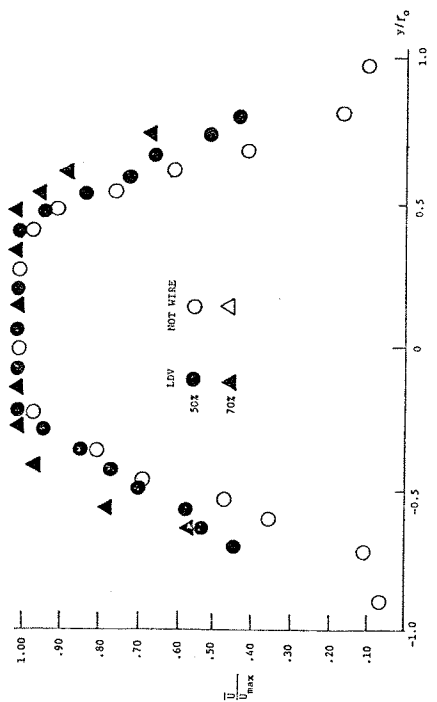


Figure 4. Mean Velocity Profile Comparison (Position II), Downstream of Venturi

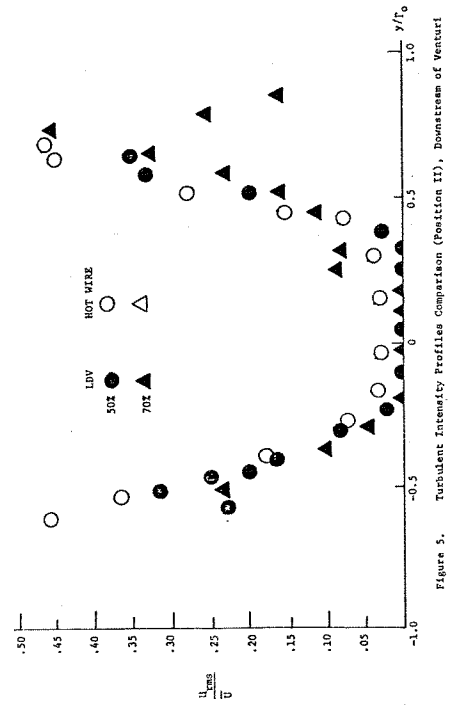


Figure 5. Turbulent Intensity Profiles Comparison (Position II), Downstream of Venturi

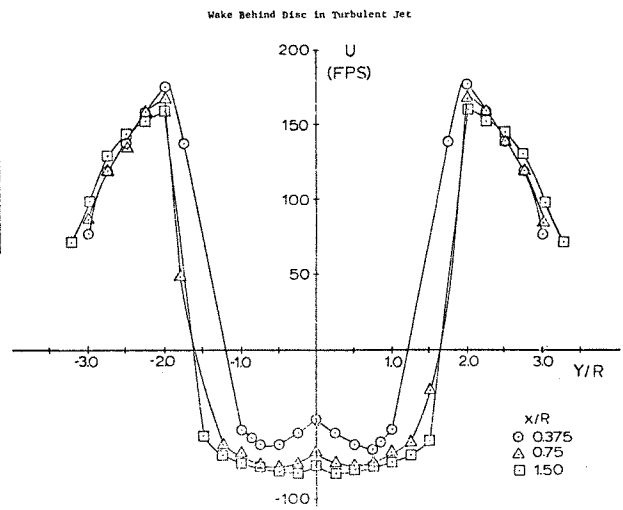
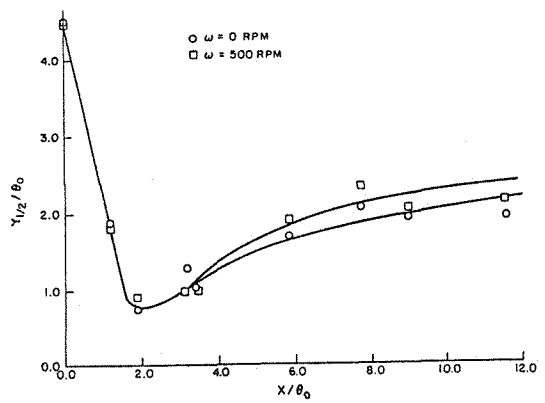
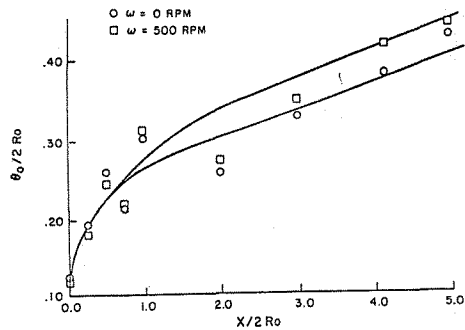
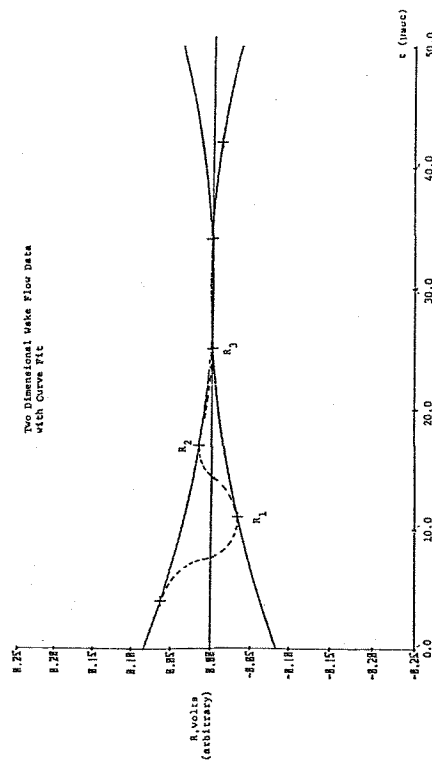
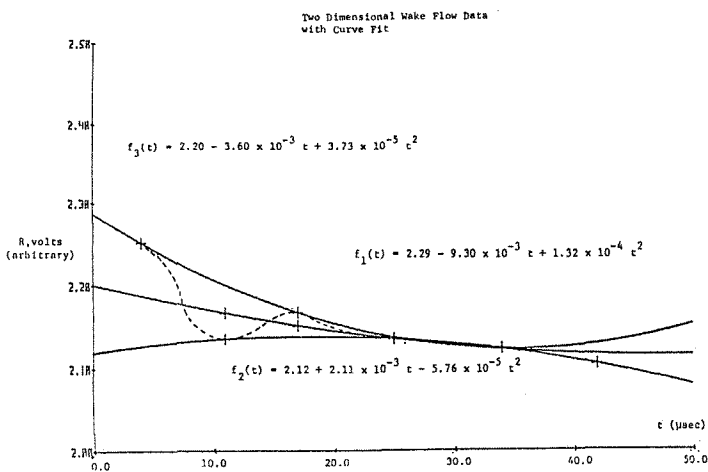
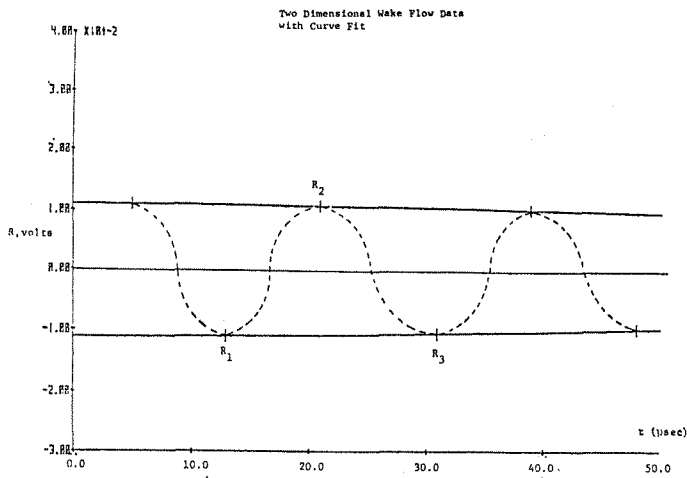
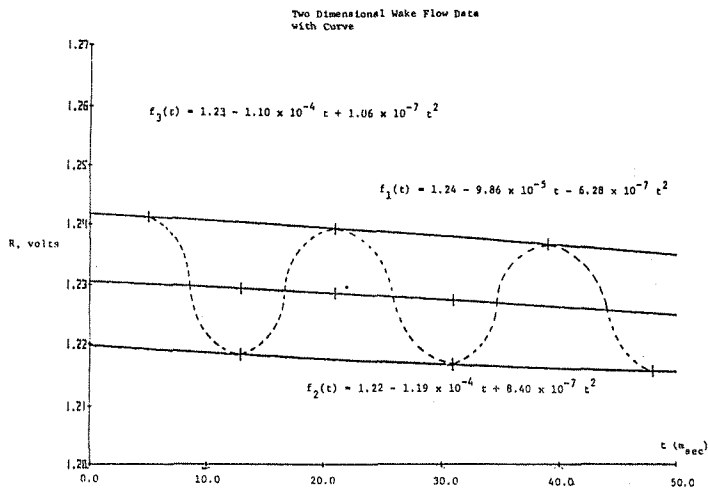


Figure 6. Mean Velocity Profiles, 2 inch Diameter Disc



Figure 7. Turbulent Intensity Profile Summary, 2 inch Diameter Disc



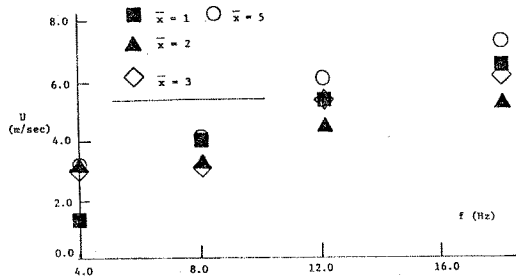


Figure 14a. Mean Velocity Development ( $y/D=0$ ) where  $\bar{X} = X/D$

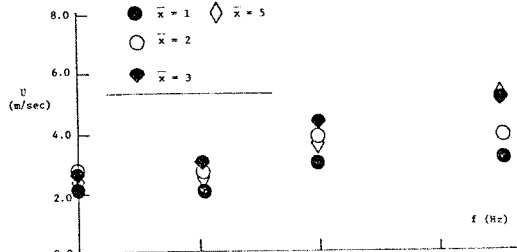


Figure 14b. Mean Velocity Development ( $y/D=1.50$ )

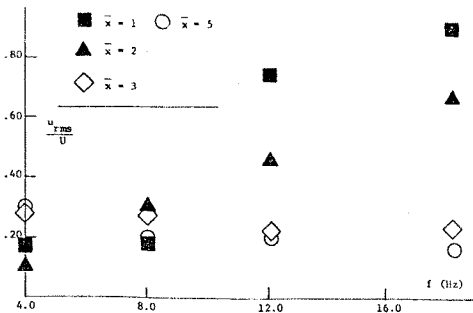


Figure 15a. Turbulent Intensity Development ( $y/D=0$ ) where  $\bar{X} = X/D$

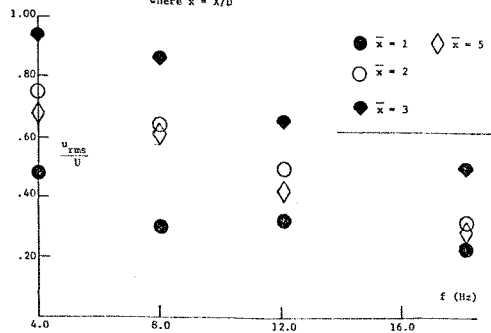


Figure 15b. Turbulent Intensity Development ( $y/D=1.5$ ) where  $\bar{X} = X/D$

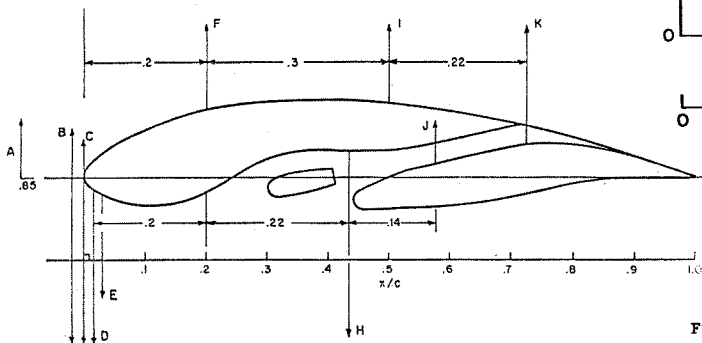


Figure 16. Two-Dimensional Ejector Wing Model with Measurement Locations

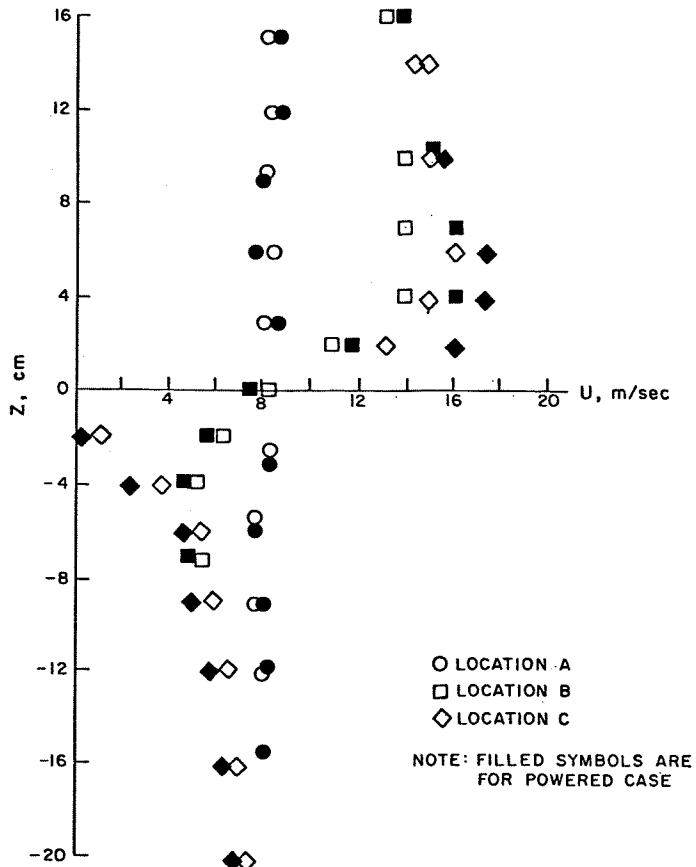


Figure 17. Mean Velocity Profiles Near the Leading Edge

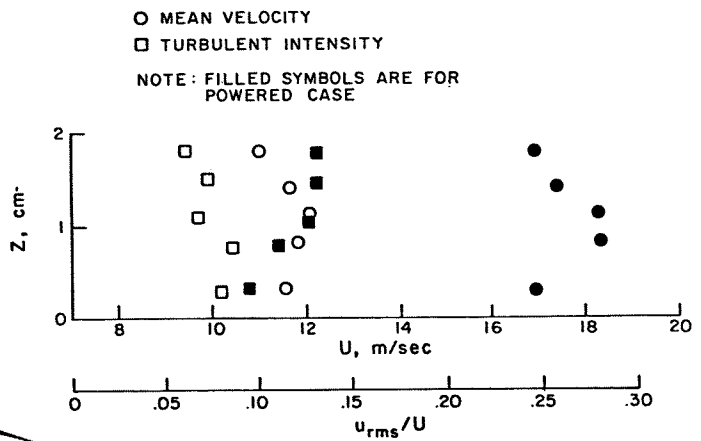


Figure 19. Mean Velocity and Turbulent Intensity Profiles in Constant Area Duct

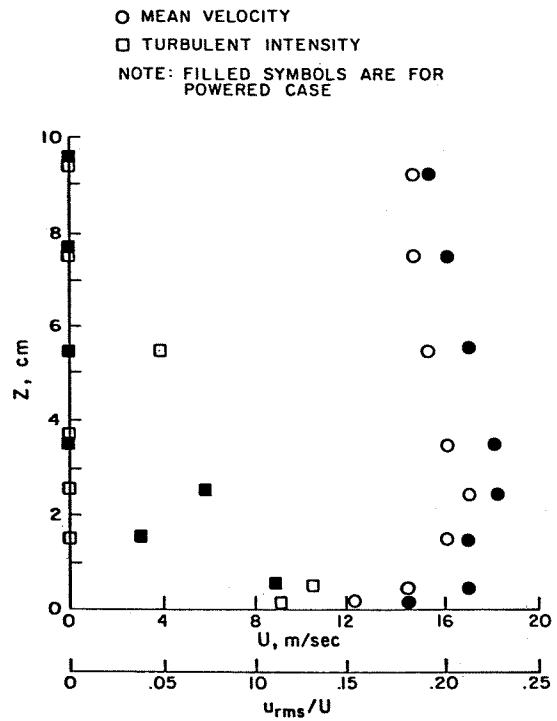


Figure 18. Mean Velocity and Turbulent Intensity Profiles above Upper Airfoil Section